Iranian Journal of Geophysics, Vol 15 No 4, 2022, Page 153 – 163 (Research Article)
DOI: 10.30499/IJG.2021.283620.1325

Fréchet Derivatives calculation for electrical resistivity imaging using forward matrix method

Reza Ghanati[1*] and Mahdi Fallahsafari[2]

[1] *Assistant Professor, Institute of Geophysics, University of Tehran, Tehran, Iran*
[2] *Ph.D Graduated, Institute of Geophysics, University of Tehran, Tehran, Iran*

(Received: 26 April 2021, Accepted: 11 October 2021)

Abstract

Fréchet derivatives calculation or sensitivity matrix is an integral part of every non-linear inversion process. The sensitivity values indicate the variation of the forward response with respect to the variation of model parameters. Sensitivity patterns are also a criterion to assess the reliability of inverted models and to design optimum resistivity surveys. In this study, a numerical approach based on the forward matrix calculation in the framework of the 2.5D finite difference electrical resistivity forward modeling is presented. First, using the potential distribution in the Fourier space obtained from the forward calculation and the derivatives of the coupling coefficients with respect to the conductivity distribution, the sensitivity values in the wavenumber domain are computed. Then, these values are transformed into the space domain using an inverse Fourier technique. To verify and analyze the proposed numerical method, the sensitivity distributions assuming the homogeneous and inhomogeneous media for commonly used electrical resistivity tomography configurations (e.g. pole-pole, pole-dipole, dipole-dipole, and the Wenner arrays) are computed. The numerical experiments reveal that the sensitivity patterns vary spatially throughout the model depending not only on the resistivity distribution but also on the electrode configuration. It is also concluded that the sensitivity analysis can be used as a supplementary tool for any optimum electrical tomography survey design.

Keywords: Electrical resistivity imaging, sensitivity function, finite difference method, wavenumber, inversion

[*] Corresponding author: rghanati@ut.ac.ir

1 Introduction

The inversion of electrical resistivity tomography provides an image of the subsurface conductivity distribution in near-surface investigations. The inverse solution of resistivity data requires knowledge about the Fréchet derivatives (sensitivity values) constructing the elements of the Jacobian matrix of the objective function. These sensitivity values denote the change in electrical potential or apparent conductivity due to a change in subsurface conductivity or resistivity distribution. The greater the value of the sensitivity function, the higher the influence of the subsurface medium on the potential measured by the electrical array. In other words, through the comparison of the derivative values for the individual data with respect to all model parameters, it is possible to give a concept of how the physical properties can be distinguished from each other by the measured surface data. Thus, the sensitivity analysis provides the possibility of optimizing field survey design and computation of resolution matrices. The dimension of the sensitivity matrix depends upon the size of the discretized model (i.e., model space) and the number of the electrode displacements so that each element of the matrix contains only the neighboring conductivities of the corresponding cell. On the other hand, for each model cell, all current sources have to be considered leading to solving $m_{\boldsymbol{d}} \times n_{\mathbf{m}}$ (where m is the number of data space and n is the number of model space) single forward problem. Hence, from the point of view of computational cost, the major implementation of electrical resistivity inversion is the sensitivity calculation. The first attempts of the Fréchet derivatives calculation for resistivity modeling are in conjunction with inversion approaches. McGillivray and Oldenburg (1990) presented a comparison of three approaches for calculating the sensitivity matrix for a 2D and 3D earth. Spitzer (1998) described derivatives for various electrode arrays at the surface and subsurface (cross-hole measurements) on 3D models using analytic and numerical schemes. An implicit formulation was proposed by Park and Van (1991) for the isotropic Fréchet derivative in the 3D case. Loke and Barker (1995) developed a numerical method for the solution of the Fréchet derivative integral on a homogeneous half-space. Zhou and Greenhalgh (1999) suggested explicit expressions for the Fréchet derivatives in terms of the Green's functions calculated with a finite element method for any cross-hole electrode array. Günther et al. (2006) used the reciprocity theorem by Geselowitz (1971) to numerically compute the sensitivity function. Szalai and Szarka (2008) dealt with sensitivity patterns in isotropic and homogeneous earth for some non-conventional arrays (non-linear arrays).

However, the above studies have been carried out based on the assumption that the subsurface structures have isotropic properties. Inclusion of the anisotropy properties results in further complexity of the inverse problem. Part of this complexity is that additional parameters must be included and solved during the inversion in what is often already an under-determined problem. Moreover, it is not always clear to specify the form of anisotropy in the starting model (Greenhalgh et al., 2009; Wiese et al., 2009). Despite successful publications for the solution of the sensitivity function, it is still an interesting research area to investigate in detail. The main motivation behind this study, in addition to providing an accurate and fast calculation approach of the sensitivity function, is to further deal with sensitivity properties of the conventional geo-electrical arrangements from the computational and theoretical aspects. Thus, a numerical

strategy based on the forward matrix method in the framework of a finite difference approach is presented. The novelty of this paper is based on the fact that a computationally time-consuming part of every electrical resistivity tomography inversion is the computation of the sensitivity matrix required to be recalculated at all iterations of the inversion process. Hence, to overcome this problem, the proposed method utilizes the results of the forward modeling computations already calculated to construct the elements of the sensitivity matrix. This strategy considerably reduces the computing time. The Fréchet derivatives of 2.5D homogeneous and inhomogeneous ground with respect to different electrical configurations are calculated. Furthermore, to reduce the computing time during the calculation of each element of the sensitivity matrix, some special tricks are taken, which will be dealt with in detail in later sections. The rest of the paper is organized as follows: Section 2 provides a detailed description of the numerical calculation of the sensitivity function. Section 3 presents the numerical results on three theoretical models for commonly used field arrays (e.g., pole-pole, pole-dipole, dipole-dipole, and the Wenner array) as well as an interpretation of the sensitivity patterns of the corresponding configurations. Finally, section 4 gives a short conclusion and summary.

2 Methodology

In general, to determine the DC sensitivity in 2.5D and 3D models, there are three numerical schemes including the adjoint equation approach, perturbation method, forward matrix technique, and one analytic method. The numerical ones are applied to arbitrary resistivity structures (inhomogeneous ground) while the analytic one is basically used for homogeneous models. Note that due to the arbitrary selection of the perturbation value, the perturbation algorithm provides an approximation to the sensitivity function in a finite difference sense. Furthermore, the computation of the entire perturbation values results in many forward calculations, which are computationally costly. Among the numerical strategies, the adjoint equation and forward matrix method are commonly utilized for the solution of the sensitivity function. In this section, to compute sensitivity with respect to an arbitrary conductivity distribution in an isotropic medium, we focus on providing a formulation of the DC forward matrix method. The governing equation of the DC electrical potential due to a point current source in 3D isotropic and inhomogeneous media is stated in terms of the partial differential equation as (Dey and Morrison, 1979; McGillivray and Oldenburg, 1990):

$$\nabla \cdot [\sigma(x.y.z)\nabla \mathrm{U}(x.y.z)] = -I\delta(x-x_s)\delta(y-y_s)\delta(z-z_s) \quad (1)$$

where I is the current intensity injected into the subsurface, σ stands for the arbitrary distribution of subsurface conductivity, δ is the Dirac delta function, U is the potential distribution due to a point source. x_s, y_s, and z_s display the position of the surface source and x, y and z indicate the position of the model cell in the discretized work area.

Taking into account the 2.5D modeling assumptions (i.e., 3D current source and 2D resistivity variation), Eq. (1) becomes:

$$\nabla \cdot [\sigma(x.z)\nabla \mathrm{U}(x.y.z)] = -I\delta(x-x_s)\delta(y-y_s)\delta(z-z_s) \quad (2)$$

To account for the 3D source characteristic, the three-dimensionality of the point source is transformed into wavenumber domain through a spatial Fourier transform of the partial differential equations along the strike direction. The corresponding

transformation of Eq. (2) yields (for more details see, e.g., McGillivray and Oldenburg,1990; Ghanati et al., 2020):

$$\nabla \cdot [\sigma(x.z)\nabla\tilde{U}(x.k_y.z) - k_y^2\sigma(x.z)\nabla\tilde{U}(x.k_y.z)] = -\frac{I}{2}\delta(x-x_s)\delta(z-z_s) \quad (3)$$

where $\tilde{U}$ denotes the transformed potential and k_y is the wavenumber with respect to the y direction. Considering a mixed-boundary condition (Dey and Morrison, 1979), the partial differential equation (Eq. 3) is solved by the method of finite difference (i.e., the central difference approximation for the partial derivatives). Hence, the numerical solution of the differential equations results in the system of algebraic equations as:

$$\boldsymbol{C}\tilde{\boldsymbol{u}}(x,k_y,z) = \boldsymbol{q} \quad (4)$$

where $\boldsymbol{C}$ is the coupling matrix affected by the subsurface conductivity distribution and discretization properties and $\boldsymbol{q}$ stands for the vector of source with the property of a discrete delta Dirac function. Note that the solution of the above symmetric and positive definite set of linear equations will give the transformed potential $\tilde{\boldsymbol{u}}(x,k_y,z)$ for specified values of k. In order to derive the potential in the spatial domain ($\boldsymbol{u}(x,z)$), the inverse Fourier transform should be applied. Since the pattern of the derivatives of the transformed potential ($\tilde{\boldsymbol{u}}$) is somewhat irregular, that is, the derivative of the transformed potential for the first wavenumber can sometimes be slightly smaller than the derivative of the transformed potential for the second wavenumber, it is not possible to use the exponential approximation for a piecewise integration in all intervals. Instead, a shape-preserving piecewise cubic interpolation algorithm is applied to approximate the integration between the smallest and largest wavenumbers. We refer to Ghanati et al. (2020) for the basics and mathematical background of 2.5D DC resistivity forward calculations.

To obtain the sensitivity quantities, it is required to differentiate Eq. (4) with respect to the n-th conductivity σ_n which yields (the source term is independent of σ_n, then $\frac{\partial \boldsymbol{q}}{\partial \sigma_n} = 0$):

$$\frac{\partial \boldsymbol{C}}{\partial \sigma_n}\tilde{\boldsymbol{u}}(x,k_y,z) + \boldsymbol{C}\frac{\partial \tilde{\boldsymbol{u}}(x,k_y,z)}{\partial \sigma_n} = 0 \quad (5)$$

For simplicity

$$\boldsymbol{C}'\tilde{\boldsymbol{u}}(x,k_y,z) + \boldsymbol{C}\tilde{\boldsymbol{u}}'(x,k_y,z) = 0 \quad (6)$$

From the above equation, with the assumption that the matrix $\boldsymbol{C}'$ is known and $\boldsymbol{C}$ and $\tilde{\boldsymbol{u}}(x,k_y,z)$ are computed from the forward calculations, the objective is to determine $\tilde{\boldsymbol{u}}'(x,k_y,z)$ on every wavenumber in the Fourier space. It is also noticed that by considering the vector $\boldsymbol{C}'\tilde{\boldsymbol{u}}(x,k_y,z)$ instead of the current vector $\boldsymbol{q}$, Eq. (6) is similar to Eq. (4).

Regarding the definition of the sensitivity matrix and Eq. (6), the derivative of the measured potential with respect to each model cell for different wavenumbers should be calculated. In addition, the capacitance matrix C consists of the coupling coefficients for all cells. However, only a number of the coupling coefficients (i.e., four elements) depend on the model cell (Appendix 1). At each of these cells, there are 3 elements that are dependent on the cording model cell. Hence, the matrix C' with the size of $n \times n$ having only twelve non-zero elements is constructed for each model parameter (Appendix 2). More details are given in Appendix 1. As a result, by using Eq. (6), the vector $\tilde{u}'$ with the size of $n \times 1$ for different wavenumbers is obtained. After deriving every wavenumber, an inverse Fourier transform is required to convert $\tilde{\boldsymbol{u}}'(x,k_y,z)$ in Fourier space to $\boldsymbol{u}'(x,z)$ in spatial space. This process is repeated for the entire model parameters (cell conductivities) giving one row of the sensitivity matrix. To complete all rows of the sensitivity matrix, the above process is implemented for each

measured voltage which totally results in $m \times n$ single forward calculations. It is noticed that the numerical effort to construct the sensitivity matrix can be considerable, in particular, when there are a large number of model parameters. To significantly reduce the computational time, it only needs to solve Eq. (6) with a specified number of rows and columns of $\boldsymbol{C}$ and $\boldsymbol{C}'$. Since the matrix $\boldsymbol{C}'$ is only a function of the geometry of the grid, the process of its computation is implemented only once for the different source locations. It is also noteworthy that during the inversion of resistivity data, it is required to simultaneously carry out the forward calculations and sensitivity matrix construction at the same code. The proposed numerical method is summarized in Algorithm 1.

Algorithm 1. Different steps of the sensitivity matrix construction
Step 1. Compute $\boldsymbol{C}'$ *(refer to Appendix 1)*
Step 2. Calculate $\boldsymbol{C}$ *using the discretization properties and conductivity distribution*
Step 3. for $i = 1$ *to* m *(*m *is number of the model parameters)*
Step 4. for $k_y = 1$ *to* p *(*p *is number of wavenumbers)*
Compute $\tilde{\boldsymbol{u}}$ *using the forward modeling*
Calculate $\tilde{\boldsymbol{u}}' = -\boldsymbol{C}^{-1}\boldsymbol{C}'\tilde{\boldsymbol{u}}$
End for
Step 5. Implement the inverse Fourier transform to obtain $\boldsymbol{u}'$
Step 6. Extract the first row of $\boldsymbol{u}'$ *to calculate the potential difference corresponding to the location of the potential electrodes*
End for
Step 7. Go to step 3 to repeat the process for all the source locations (The numerical results presented in this study are based on the derivative of only one measured potential (or source location) with respect to the entire model cells, that is, construction of merely one row of the sensitivity matrix).

It should be also noted that if step 8 is carried, to convert $\boldsymbol{u}' = \frac{\partial \boldsymbol{u}}{\partial \sigma}$ into $\frac{\partial \rho_a}{\partial \rho}$, which is used in the inversion process as the Jacobian matrix, it is required to multiply $\boldsymbol{u}'$ by the factor $\frac{K}{I} \times (-\sigma^2)$, where K, I and σ are the geometry factor, current intensity, and conductivity, respectively (for more details see Appendix 1).

3 Numerical experiments

In this section, the sensitivity patterns of one homogeneous model and two inhomogeneous models, including a three-layered earth and a rectangular body buried in a high resistive half-space medium, with respect to different electrical arrays, e.g. pole-pole, pole-dipole, dipole-dipole and the Wenner arrays are presented. We used the same gridding and forward calculations for all models and electrode arrays, with a grid size equal to the minimum electrode distance in the x-direction. The grid model contains 20×78 regular cells (rectangular blocks) in vertical and horizontal directions, respectively. This number of cells also includes the boundary conditions (i.e., cells corresponding to both left and right sides and surface and bottom boundaries). Note that the discretized model is divided into two regions: work area or area of interest with a much finer grid to ensure accurate results and extended area with a coarse grid.

i) Homogeneous half-space model

Fig. 2 shows the sensitivity pattern of a homogeneous half-space model of 50 Ωm represented in Fig. 1-a for different configurations. The maximum depth of investigation associated with pole-pole, pole-dipole, dipole-dipole, and the Wenner arrays are computed based on Edwards (1977). From the numerical results, it is noticed that for all the configurations, the highest sensitivity values are found near both the potential

and current electrodes. At larger distances from the electrodes, the contour patterns are different for different arrays. The difference in the contour pattern of the sensitivity function plot helps to explain the response of the different arrays to different types of structures. In addition, the effective depth of measurement is sequentially increased by increasing the distance between the receiving electrodes and the transmitting electrodes. The farther is distance, the greater is the vertical interval in which the bulk of the current flows. One important observation can be made when considering the sensitivity sections, that is, the negative sensitivity between the source electrode and receiving electrode and positive sensitivity between the source and potential electrode pairs.

Fig. 2-a indicates the sensitivity plot corresponding to the pole-pole array. Comparing the sensitivity patterns, it is observed that this array has the widest horizontal coverage and the deepest depth of investigation. However, it has the poorest resolution, which is reflected by the comparatively large spacing between the contours in the sensitivity function plot. The asymmetrical nature of the pole-dipole array is evident in the sensitivity section which is due to a remote current electrode (see Fig. 2-b). From the sensitivity function, it is

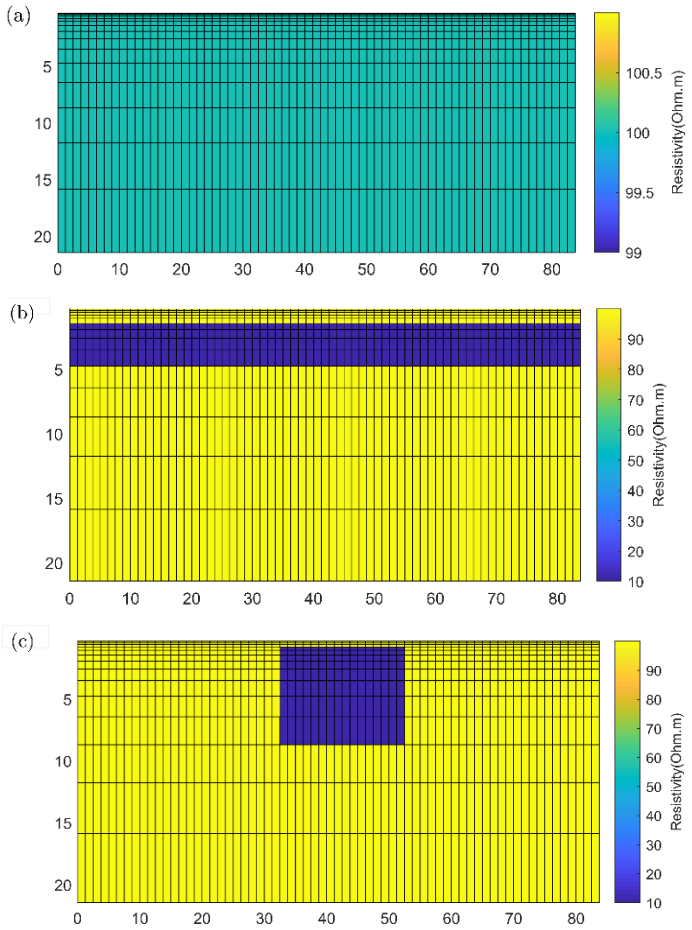

Fig 1. Representation of the simulated structures (a) homogeneous half-space model (b) three-layered model (c) rectangular body model.

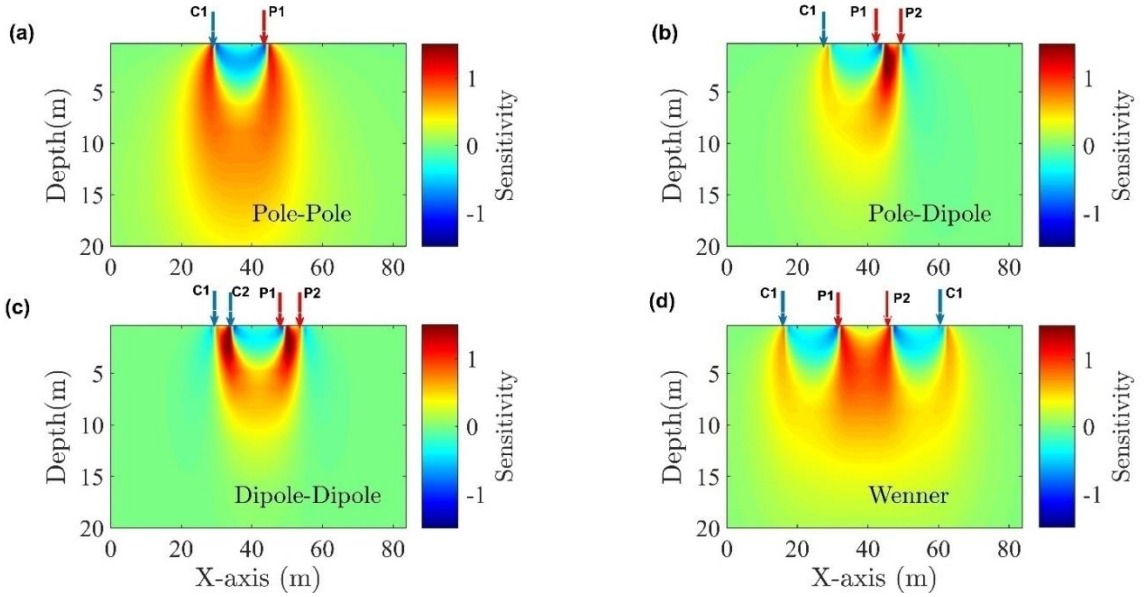

Fig 2. Normalized sensitivity patterns associated with a homogeneous half-space of 100 Ωm for (a) pole-pole (b) pole-dipole (c) dipole-dipole (d) the Wenner arrangement with electrode spacing of 5 m and $n = 3$ (n is the number of receiver-transmitter separation). The blue and red arrows represent the location of current and potential electrodes.

obvious that analogous to dipole-dipole, this array has almost vertical contours, but a larger depth of investigation compared to the dipole-dipole array. For the pole-dipole array with large receiver-transmitter separation, the region with the highest positive sensitivity values concentrates below the potential electrode pair. Referring to Fig. 2-c, the dipole-dipole array has almost vertical contours beneath the center of the array meaning that the dipole-dipole configuration is more sensitive to vertical structures than to horizontal structures. Contrary to the dipole-dipole array, the sensitivity pattern of the Wenner array is almost horizontal leading to better detection of horizontal anomalies, but poor recognition of vertical anomalies (see Fig. 2-d).

ii) Three-layered model

To deal with the influence of inhomogeneity on the sensitivity pattern, an inhomogeneous structure including a three-layered earth ($\rho_1 = 100$, $\rho_2 = 10$, $\rho_3 = 100$) represented in Fig. 1-b is considered. The numerical results are shown in Fig. 3, which indicates the sensitivity patterns for a fixed transmitter/source combination in terms of different electrical configurations. From this figure, it can be seen that the presence of inhomogeneity in the medium introduces the asymmetry into the sensitivity pattern. Furthermore, the Wenner array shows better vertical resolution, which confirms its superiority over the other arrays for detection of the layered structures. It is also seen that the dipole-dipole and pole-dipole arrays show less sensitivity to the layered earth model due to the poor vertical resolution of the dipole package (i.e. pole-dipole and dipole-dipole).

iii) Rectangular body model

The second inhomogeneous example includes one embedded block with the resistivity of 10 Ωm buried in 100 Ωm half-space at 1.2 m from the ground surface (Fig. 1-c). The object of this example is to investigate the sensitivity function of different arrays with respect to vertical structures. From Fig. 4, it is observed that the sensitivity pattern illustrates large negative values near the surface between C_1 and P_1 electrodes, as well as between C_2 and P_2 electrodes. This means that if a small body with a

higher resistivity than the background medium is placed in these negative zones, the measured apparent resistivity value will decrease. On the contrary, if the high resistivity body is placed between P_1 and P_2 electrodes, where there are large positive sensitivity values, the measured apparent resistivity will increase. It is also concluded that the presence of inhomogeneity causes the distortion of the sensitivity pattern compared to a homogeneous medium. In addition, our numerical experiments demonstrate that the dipole-dipole and pole-dipole configurations have almost vertical contours indicating its higher sensitivity to vertical structures than to horizontal structures.

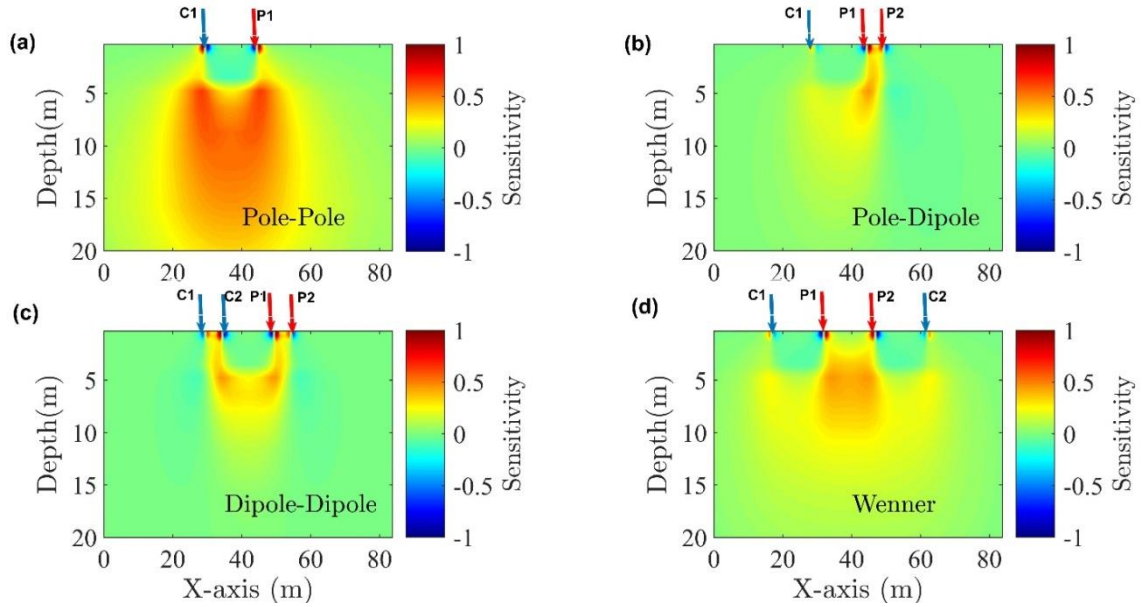

Fig 3. Normalized sensitivity patterns associated with a three-layered model ($\rho_1 = 100\ \Omega m$, $\rho_2 = 10\ \Omega m$, $\rho_3 = 100\ \Omega m$) for (a) pole-pole (b) pole-dipole (c) dipole-dipole (d) the Wenner arrangement with electrode spacing of 5 m and $n = 3$ (n is the number of receiver-transmitter separation). The blue and red arrows represent the location of current and potential electrodes.

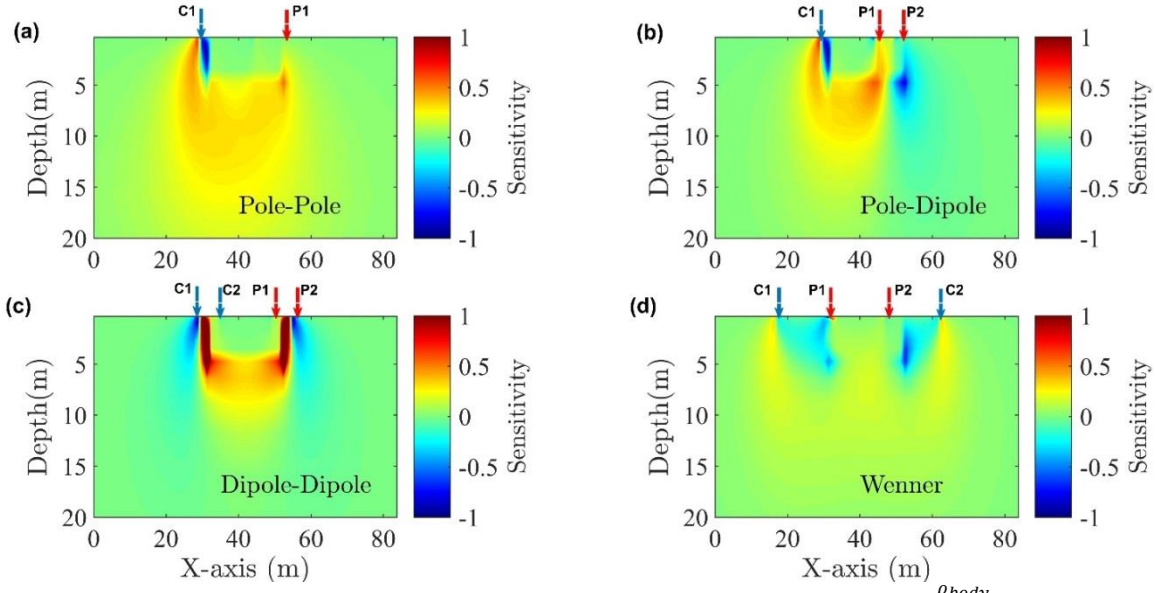

Fig 4. Normalized sensitivity patterns associated with a rectangular body model ($\frac{\rho_{body}}{\rho_{background}} = 0.1$) for (a) pole-pole (b) pole-dipole (c) dipole-dipole (d) the Wenner arrangement with electrode spacing of 5 m and $n = 3$ (n is the number of receiver-transmitter separation). The blue and red arrows represent the location of current and potential electrodes.

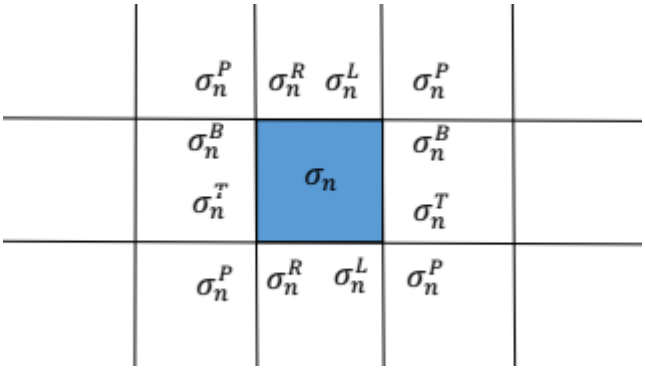

Fig 5. The model cell σ_n and twelve coupling coefficients depending on σ_n. P, B, R, and L stand for the central, bottom, right and left nodes, respectively.

4 Conclusions and Remarks

An accurate and fast sensitivity calculation technique is the basis of any efficient electrical resistivity tomography inversion. Therefore, we proposed and formulated a numerical method using the element stiffness matrices and the potential distribution obtained from the finite difference modeling to calculate the sensitivity matrix values. The sensitivity distribution was computed for 2.5D electrical resistivity modeling in terms of different surface electrical configurations. The sensitivity function determines the degree to which a change in the conductivity of a section of the subsurface will influence the potential measured by an electrical array. To verify the proposed numerical algorithm, the sensitivity patterns of one homogeneous and two inhomogeneous models were provided. In general, using the numerical experiments, it was demonstrated that the difference in the contour pattern of the sensitivity function plot helps to explain the response of different arrays to different types of structures and to determine the relative merits (e.g., resolution and penetration depth) of using some of the configurations for resistivity imaging. From our numerical experiments, it was shown that: 1) the pole-pole array has the maximum penetration depth but the lowest horizontal and vertical resolution; 2) contrary to the pole-dipole and dipole-dipole configurations, the Wenner array is more sensitive to vertical changes than to horizontal changes, that is, the horizontal structures would be better detected by the Wenner array; 3) deformation of the sensitivity distributions is inevitable in the presence of inhomogeneity. Using the numerical strategy proposed in this study, the sensitivity function associated with any arbitrarily inhomogeneous cases can be calculated with the aim of resolution studies, experimental design of a survey and updating of model parameters during an inversion.

Acknowledgements

The authors are grateful to anonymous reviewers for their constructive and fruitful comments, which helped to significantly improve the clarity of this paper. We also thank the University of Tehran for all its support.

References

Dey, A., and Morrison, H. F., 1979, Resistivity modelling for arbitrarily shaped two-dimensional structures: Geophysical Prospecting, **27**(1), 106-136.

Edwards L. S., 1977, A modified pseudosection for resistivity and IP. Geophysics, **42**, 1020–1036.

Geselowitz, D. B., 1971, An application of electrocardiographic lead theory to impedance plethysmography: IEEE

Transactions on Biomedical Engineering, **18**(1), 38–41.

Ghanati, R., Azadi, Y., and Fakhimi, R., 2020, RESIP2DMODE: A MATLAB-based 2D resistivity and induced polarization forward modeling software: Iranian Journal of Geophysics, **13**(4), 60-78.

Greenhalgh, S. A., Zhou, B., Greenhalgh, M., Marescot, L., and Wiese, T., 2009, Explicit expressions for the Fréchet derivatives in 3D anisotropic resistivity inversion: Geophysics, **74**, F31-F43.

Günther, T., Rücker, C., and Spitzer, K., 2006., Three-dimensional modelling and inversion of DC resistivity data incorporating topography – II, Inversion: Geophys. J. I., **166**, 506–517.

Loke, M. H., and Barker, R. D., 1995, Least-squares deconvolution of apparent resistivity pseudosections: Geophysics, **60**, 1682–1690.

McGillivray, P. R., and Oldenburg, D. W., 1990, Methods for calculating Fréchet derivatives and sensitivities for the non-linear inverse problem: a comparative study: Geophysical Prospecting, **38**(5), 499–524.

Park, S. K., and Van, G. P., 1991, Inversion of pole-pole data for 3-d resistivity structure beneath arrays of electrodes: Geophysics, **56**, 951–960.

Spitzer, K. 1998, The three-dimensional DC sensitivity for surface and subsurface sources: Geophys. J. I., **134**(3), 736–746.

Szalai, S., and Szarka, L., 2008, Parameter sensitivity maps of surface geo-electric arrays I. Linear arrays: Acta Geodaetica et Geophysica, **43**, 419–437.

Wiese, T., Greenhalgh, S., and Marescot, L., 2009, DC resistivity sensitivity patterns for tilted transversely isotropic media: Near Surface Geophysics, **7**(2), 125–139.

Zhou, B., and Greenhalgh, S. A., 1999, Explicit expressions and numerical computation of the Fréchet and second derivatives in 2.5D Helmholtz equation inversion: Geophysical Prospecting, **47**, 443–468.

Appendix 1

As stated in section 3, a part of the equation of the sensitivity function is the derivative of the coupling matrix $\boldsymbol{C}$ with respect to σ_n, where n is the number of model parameters (model cells), i.e., $\frac{\partial \boldsymbol{C}}{\partial \sigma_n}$. The matrix $\frac{\partial \boldsymbol{C}}{\partial \sigma_n}$ with twelve non-zero elements has the size of $n_z \times n_x \times n_z \times n_x$, where n_z and n_x are the number of model cells in the z and x directions, respectively. Fig. 5 shows the elements of $\boldsymbol{C}$ which are dependent on σ_n. For more details of the structure of the coupling matrix, the reader is referred to Dey and Morrison (1979). Furthermore, an open-source Matlab code has been provided by Ghanati et al. (2020) in which the matrix $\boldsymbol{C}$ is constructed by a Matlab script named 'Potantialinitial.m'.

In addition, based on the cells and coupling coefficients affected by a change in the model cell σ_n, the matrix $\boldsymbol{C}'$ is:

$$\frac{\partial \boldsymbol{C}}{\partial \sigma_n} = \begin{bmatrix} 0 & 0 & & & \cdots & & & 0 & 0 \\ 0 & \ddots & & & & & & \iddots & 0 \\ & & \frac{\partial \boldsymbol{C}_P}{\partial \sigma_n} & \frac{\partial \boldsymbol{C}_B}{\partial \sigma_n} & & \frac{\partial \boldsymbol{C}_R}{\partial \sigma_n} & 0 & & \\ & & \frac{\partial \boldsymbol{C}_T}{\partial \sigma_n} & \frac{\partial \boldsymbol{C}_P}{\partial \sigma_n} & & 0 & \frac{\partial \boldsymbol{C}_R}{\partial \sigma_n} & & \\ \vdots & & & & \ddots & & & & \vdots \\ & & & & & \frac{\partial \boldsymbol{C}_P}{\partial \sigma_n} & \frac{\partial \boldsymbol{C}_B}{\partial \sigma_n} & & \\ & & \frac{\partial \boldsymbol{C}_L}{\partial \sigma_n} & 0 & & \frac{\partial \boldsymbol{C}_T}{\partial \sigma_n} & \frac{\partial \boldsymbol{C}_P}{\partial \sigma_n} & & \\ 0 & \iddots & 0 & \frac{\partial \boldsymbol{C}_L}{\partial \sigma_n} & & & & \ddots & 0 \\ 0 & 0 & & & \cdots & & & 0 & 0 \end{bmatrix}$$

Appendix 2

This appendix explains how to calculate $\frac{\partial \rho_a}{\partial \rho}$ from $\frac{\partial \boldsymbol{u}}{\partial \sigma}$.

First, we calculate $\frac{\partial \rho_a}{\partial \sigma} = \frac{\partial \boldsymbol{u}}{\partial \sigma} \times \frac{K}{I}$ (analogous to $\rho_a = u \times \frac{K}{I}$).

Then using the chain rule, we have:

$$\frac{\partial \rho_a}{\partial \sigma} = \frac{\partial \rho_a}{\partial \rho} \times \frac{\partial \rho}{\partial \sigma} = \frac{\partial \rho_a}{\partial \rho} \times (-\rho^2)$$

$$\frac{\partial \rho_a}{\partial \rho} = \frac{\partial \rho_a}{\partial \sigma} \times (-\sigma^2) = \frac{\partial u}{\partial \sigma} \times \frac{K}{I} \times (-\sigma^2)$$

where ρ_a is the apparent resistivity. ρ indicates the true resistivity and u stands for the electrical potential distribution. K, I and σ are the geometry factor, current intensity and conductivity, respectively.